Fuel 348 (2023) 128475

Contents lists available at ScienceDirect

Fuel

journal homepage: www.elsevier.com/locate/fuel

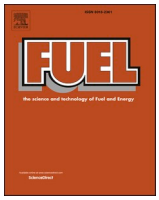

Full Length Article

Synergistic effects of nanosecond plasma discharge and hydrogen on ammonia combustion

Mohammad Shahsavari [a,*], Alexander A. Konnov [b], Xue-Song Bai [c], Agustin Valera-Medina [d], Tie Li [e], Mehdi Jangi [a]

[a] Department of Mechanical Engineering, University of Birmingham, United Kingdom
[b] Division of Combustion Physics, Department of Physics, Lund University, Sweden
[c] Division of Fluid Mechanics, Department of Energy Science, Lund University, Sweden
[d] College of Physical Science and Engineering, Cardiff University, United Kingdom
[e] Institute of Power Plants and Automation, Shanghai Jiao Tong University, PR China

ARTICLE INFO

Keywords:
Ammonia/hydrogen combustion
Plasma-assisted combustion
Nanosecond-pulsed plasma discharge

ABSTRACT

Synergistic effects of nanosecond plasma discharge and hydrogen on the combustion characteristics of ammonia/air are numerically studied under conditions relevant to gas turbine combustion chambers. It is shown that increasing the plasma contribution in assisting the flame results in lower NO_X emissions by up to 27% than those in flames assisted by hydrogen for the range of operating conditions considered in this study. Plasma makes the consumption speed of the reactants less prone to the strain rate than that in flames assisted by hydrogen. It is found that discharging plasma with the pulse energy density of 9 mJ/cm^3 alongside using 12% hydrogen by volume in the fuel increases the flame speed of ammonia/air to those of conventional fossil fuels such as methane—an improvement that is not achievable by just using hydrogen, even at a high concentration of 30%. Furthermore, raising the pulse energy density beyond a specific value broadens the reaction zones by generating radical pools in the flame preheating zone, which is expedited in fuel-rich conditions with high H_2 fuel fractions. Investigations show that the simultaneous utilization of high-energy plasma and hydrogen reduces the NO_X emissions by activating the mechanisms of nitrogen oxide denitrification ($DeNO_X$) in preheating and post-flame zones, being more significant under the lean condition as compared with rich and stoichiometric cases. It is shown that increasing mixture pressure significantly deteriorates the impacts of plasma on combustion. Such unfavorable effects are weakly controlled by changes in the reduced electric field caused by pressure augmentations.

1. Introduction

Hydrogen carriers have become a viable source of energy in the face of increasingly stringent environmental legislation enacted to reduce greenhouse gas emissions. Unfortunately, utilizing some of these energy carriers, e.g., pure hydrogen, on an industrial scale is burdened with strenuous and expensive production, storage, and transportation technologies. Ammonia is known as one of the promising alternatives at hand, thanks to its well-established mass production and utilization as a fertilizer in agricultural sectors [1]. Nevertheless, the direct combustion of pure ammonia in conventional combustors is dismayed by its relatively lower reactivity than that of typical hydrocarbon fuels [2].

Co-burning ammonia with highly reactive fuels is considered a practical method to enhance the reactivity of ammonia [3–8]. However, utilizing ammonia as a dual fuel or a blend mixed with other hydrocarbon fuels compromises the advantages of ammonia as a carbon-free fuel since a considerable amount of hydrocarbon fuels is needed to stabilize ammonia flames [9]. Hydrogen is one of the best carbon-free additives to enhance ammonia combustion thanks to its substantial reactivity [10,11]. Extensive valuable studies have addressed this topic in the literature [12–17], which showed that a noticeable volume fraction of hydrogen in the blend, e.g., 20–50%, is required to burn ammonia in engines properly [14]. Wiseman *et al.* showed that a mixture comprised of 45% of H_2 by volume in NH_3/N_2 considerably reduces the susceptibility of the flame to blow out due to the fast preferential diffusion of hydrogen into the preheating layer [11]. Nevertheless,

* Corresponding author.
E-mail address: m.shahsavari@bham.ac.uk (M. Shahsavari).

https://doi.org/10.1016/j.fuel.2023.128475
Received 5 December 2022; Received in revised form 23 March 2023; Accepted 17 April 2023
Available online 26 April 2023

increasing the hydrogen volume fraction in the range of 0–30% in fuel-lean mixtures substantially increases the NO_X emissions [13,14], which would be due to a larger quantity of OH radicals in the NH_3/H_2 flames compared with that of pure ammonia flames [18,19]. Burning NH_3/H_2 blends under very lean conditions may result in thermoacoustic instabilities, flame instabilities, and noticeable NO and N_2O emissions [13,20,21], while burning fuel-rich mixtures results in incomplete combustion [13]. Therefore, co-burning ammonia with hydrogen is a trade-off between combustion stability and pollutant emissions. Preheating the fresh mixture is another method for assisting ammonia flames [22,23]. However, NH_3/Air mixtures must be preheated by a few hundred degrees Kelvin to stabilize the flame and prevent incomplete combustion [22,23].

Plasma is a promising method to assist combustion [24,25]. A commendable number of investigations have been carried out to elucidate the impacts of plasma on combustion by focusing on widely used fuels, e.g., CH_4 [26–28] and H_2 [29–33]. These investigations showed that plasma could assist combustion by accelerating fuel dissociation [26], increasing radical pools [30], and raising the mixture temperature [31]. Recently, this novel method has been applied to ammonia combustion. Faingold *et al.* [34,35] utilized zero-dimensional simulations to evaluate the impact of nanosecond plasma discharge (NSD) on the ignition delay time (IDT) of ammonia. They showed that the required number of pulses and plasma repetition frequency to substantially assist ammonia ignition are highly dependent on the initial mixture temperature [34]. Taneja *et al.* numerically studied plasma-assisted ammonia combustion [36]. They indicated that ignition delay time drops proportionally by raising the pulse frequency and energy density per pulse. They also showed that pressure-dependent recombination reactions delay the ignition by reducing the reactive radicals at high-pressure conditions [36]. In a brief communication, Choe *et al.* reported that NSDs could improve the lean blowout limit and reduce NO_X emissions in NH_3/Air flames [37]. Similar findings have also been reported by Lin *et al.* [38], Kim *et al.* [39], and Tang *et al.* [40] for a range of NH_3/Air flames assisted by high-energy gliding arc plasma, dielectric barrier discharges, and AC powered gliding arc discharges, respectively. Our recent study showed that NO_X emissions in plasma-assisted ammonia flames change non-monotonically with the level of pulse energy density, E_p [41]. NO_X emissions noticeably increase by discharging low-energy NSDs in ammonia flames. Increasing E_p beyond a specific value, e.g., 17 mJ/cm^3 for $NH_3/O_2/N_2$ with an equivalence ratio of 0.8 and an initial fresh mixture temperature of 850 K, accelerates the NO consumption rate [41], which would finally result in considerable NO_X reduction at very high pulse energy densities. Our investigations also showed that increasing the plasma energy alters the preheat zone of ammonia flames toward the flameless mode of combustion [41].

Utilizing plasma and hydrogen is known as the best assessment for ammonia combustion to date. The above-mentioned studies have shown that each of these methods can enhance the IDT and flame speed (S_L) of ammonia. Nevertheless, there is no data publicly available in the literature comparing these methods in assisting ammonia combustion. Besides, to the best of the authors' knowledge, the synergistic effects of plasma and hydrogen on ammonia combustion have not been addressed in the literature. By using numerical simulations, the main objectives of the present paper are to compare plasma and hydrogen and to evaluate the synergistic effects of these methods on the characteristics of ammonia flames, e.g., IDT, S_L, flame thickness (FT), extinction strain rate (κ_e) and NO_X emissions.

2. Numerical method and settings

2.1. Numerical solver

Non-equilibrium plasma-assisted combustion was modeled by coupling the open-source Boltzmann equation solver, ZDPlaskin [42], with Cantera [43] codes. The former solves the chemical reaction during the plasma discharge, while the latter codes integrate the ODEs of thermal reactions. This two-way coupling was set up to resolve plasma-combustion interactions accurately. This methodology is computationally affordable in zero- and one-dimensional simulations. However, utilizing this two-way coupling in three-dimensional CFD simulations would require mapping the chemical kinetic mechanisms to a lower dimensional thermodynamic space to speed up the numerical integration of the chemical reaction rates [44,45]. Here, IDT was calculated in an adiabatic constant-volume reactor coupled with ZDPlaskin (Fig. 1 (a)). As schematically shown in Fig. 1(b), to obtain laminar premixed flame characteristics, i.e., S_L, FT, κ_e, and pollutant emissions, the fresh mixture is first stimulated by 20 NSDs in an adiabatic constant-pressure reactor in Cantera coupled with ZDPlaskin. Here, the number of pulses was selected based on the typical flow residence time between plasma dielectrics. Furthermore, plasma is discharged upstream of the flame in the fresh reactant, an effective location to assist a premixed flame [46]. Then, the stimulated mixture from the constant-pressure reactor was used as the reactants for the one-dimensional freely-propagating flame and twin premixed flame models to simulate unstrained and strained premixed flames, respectively. In Fig. 1, T is temperature, $[X_i]$ is species molar concentration, P is pressure, V is volume, and the subscript "u" shows reactant specifications in one-dimensional freely propagating flame and twin premixed flame models. The plasma discharge was modeled by a square-shaped wave, as shown in Fig. 2. The integration time steps were specified by using an adaptive temporal refining method to accurately resolve reactions with a broad range of timescales, from picosecond electron impact reactions to microsecond thermal reactions. A schematic of the adaptive method can be found in Fig. 2.

2.2. Kinetic models

The kinetics of ammonia/hydrogen oxidation was modeled by using the mechanisms developed by Han *et al.* [47,48]. These kinetic models include reactions of excited species, such as $O_2(a^1\Delta g)$ and $O(^1D)$ [49]. The previous study by Gotama *et al.* [10] showed that the mechanism published in [47] can accurately predict the laminar burning velocity of NH_3/H_2/air mixtures for the range of equivalence ratios, i.e., $0.8 < \phi < 1.3$ and $0.8 < \phi < 1.05$, at $p = 1$ and 5 bar, respectively. Our previous studies also showed this mechanism precisely predicts the ignition delay time of ammonia/air [41]. However, as it can be found from the details presented in the Supplementary Materials (Fig. S1), the latest version of the Han *et al.* mechanism [48] predicts the extinction strain rates of ammonia/air more accurately than the one published in [47]. Therefore, the latest version of the Han *et al.* mechanism [48] is used here to study the effects of plasma discharge on extinction strain rates, while other flame properties were obtained by utilizing the mechanism provided in [47].

Here, a plasma kinetic mechanism was developed by combining the mechanism presented by Faingold *et al.* for NH_3/O_2/He [34] with the plasma reactions for N_2 and H_2 from the study of Zhong *et al.* [50] and Mao *et al.* [51], respectively. The electron-species collision cross-sections were obtained from the LXCat database [52]. The developed plasma kinetic model comprises 790 elementary reactions, including excitations, ionizations, quenching, recombination, charge exchanges, and neutral state reactions for $NH_3/H_2/O_2/N_2$ mixtures. Kinetic models and the utilized collision cross-sections can be found in the Supplementary Materials.

2.3. Modeling parameters

In this study, equivalence ratio, ϕ, and pressure, p, were varied in the range of 0.8–1.2 and 1–5 atm, respectively. The initial mixture temperature, T_{in}, was kept constant at 850 K, at which the ammonia oxidation rate is considerably slow and weak without using plasma or hydrogen [41,53]. To compare the effects of NSD and hydrogen with those of pure preheating on ammonia combustion, characteristics of

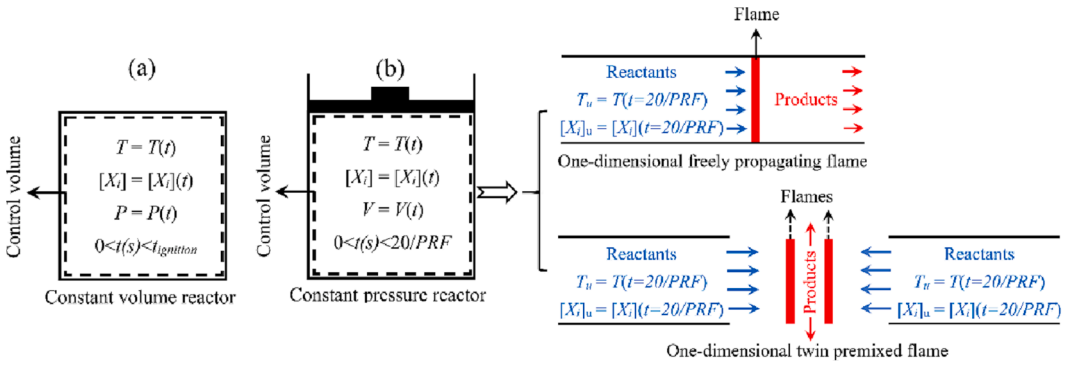

Fig. 1. Schematic of (a) constant-volume reactor and (b) constant-pressure reactor coupled with one-dimensional freely-propagating flame and a twin premixed flame models.

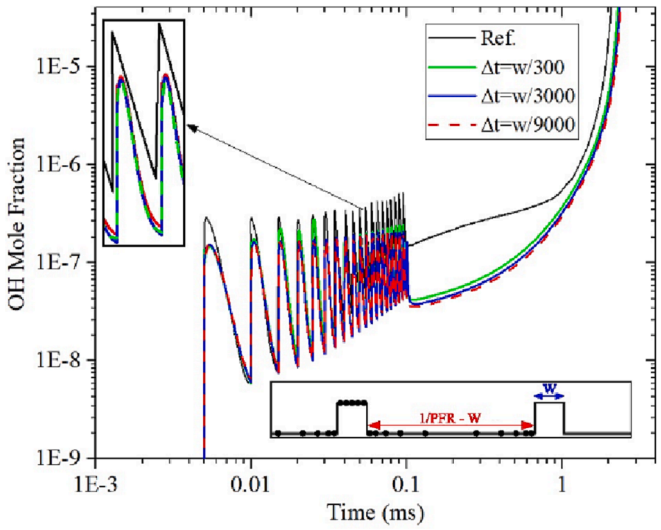

Fig. 2. Temporal evolution of OH mole fraction in plasma-assisted NH_3/O_2/He ignition at $\phi = 1$, $T_{in} = 1500$ K, and $p = 1$ atm with $PRF = 200$ kHz and $E/N = 180$ Td.

NH_3/air flames were also calculated by elevating the fresh mixture temperature, initially at 850 K, by $0 < \Delta T < 700$ K. Understanding the ammonia flame behavior at extreme preheated conditions is important due to its prolonged ignition delay time. This is of particular interest in the case of ammonia flames in internal combustion engines, wherein the co-existence of the flame and ignition modes can largely impact the late stage of the heat-release and burning of the near-wall mixtures, thereby, the overall engine performance as discussed in references [54–57]. The mole fraction of oxygen in the oxidizers was kept constant at 0.21 in all the simulations, while the mole percentage of hydrogen in the fuel, X_{H2}, defined in Eq. (1), was altered in the range of 0–35%.

$$X_{H2} = 100 \times \frac{x_{H_2}}{x_{NH_3} + x_{H_2}} \quad (1)$$

where, x_{H2} and x_{NH3} are the mole fractions of H_2 and NH_3, respectively. Here, the concentration of neutrals, N, in the reactants was calculated by obtaining the density of species and the mixture by utilizing the ideal gas equation of state.

In this study, non-equilibrium NSD was used to assist ammonia flames, which is known as the most energy-efficient plasma technology [26,30]. Plasma settings were chosen based on non-thermal plasma generators utilized in the literature [32,53]. In each simulation, 20 plasma pulses were discharged with the pulse repetition frequency, PRF, of 50 kHz and the reduced electric field, E/N, of 350 Td. Our previous studies showed that NSDs have the most pronounced effects on the combustion characteristics of ammonia/air when the reduced electric field is set at 350 Td [41]. For plasma-assisted pressurized mixtures, plasma settings were set based on N, i.e., the electric field constant, E, was calculated based on the specified E/N and calculated N. Simulations were also performed by keeping E constant, in which E/N was updated during each iteration based on N. The pulse energy density, E_p, was varied in the range of 0–10 mJ/cm^3 to study the effects of pulse energy on plasma-assisted combustion. The utilized E_p values are in the range of the ones used in the literature [26,32,34,38,50,57–59], for which the number density of electrons is always less than 10^{14}cm^{-3} while the electron temperature is 5 eV. This indicates that the plasma is in the non-thermal (cold) phase [60]. Here, an adaptive pulse width, w, was used to ensure that the specified E_p was released during each pulse.

3. Validations

Despite the valuable investigations that delved into ammonia combustion in the past, no experimental data are available in the literature about the time history of species mole fractions or temperature for plasma-assisted ammonia combustion. In this light, the present numerical solver was first validated against Faingold *et al.* numerical results on plasma-assisted $NH_3/He/O_2$ ignition at $\phi = 1$ and $p = 1$ atm [34]. These validation results were also presented in our previous study on plasma-assisted ammonia combustion [41]. Comparisons presented in Fig. 2 show that the present numerical results are in good agreement with those of reference [34]. However, the OH mole fraction during the pulses and in the post-plasma phase, i.e., time > 0.1 ms, obtained here, is lower than that reported in the reference. Such discrepancies are not due to the numerical resolutions, as efforts were made in the present study to obtain temporal resolution-independent results by varying the time step size, Δt, as can be seen in Fig. 2. It should be noted that the details of the numerical method and initial conditions are not provided in reference [34]. Thus, the discrepancies could be attributed to the use of different initial conditions. In the present study, the initial number density of electrons was set at 1 cm^{-3}, while other radicals, charged and electronically excited species, were set to zero at the initial conditions.

Further model validations were carried out by reproducing the experimental data obtained by Lefkowitz *et al.* on plasma-assisted CH_4/O_2/He mixtures with 75% dilution [60]. To such an aim, the plasma kinetic mechanism developed by Mao *et al.* comprised of 629 reactions, was used [28]. Fig. 3 shows the temporal distribution of temperature during and after 300 NSDs with the $PFR = 30$ kHz and $E/N = 180$ Td in a constant-volume reactor. The initial mixture temperature and pressure are 300 K and 60 Torr, respectively. Here, a similar heat loss term as that used in reference [61] was added to the energy equation to include the conduction heat transfer to the dielectrics. The uncertainty of the experimental data reported by Lefkowitz *et al.* [61] is also shown in Fig. 3. Simulations were carried out with different Δt values to achieve

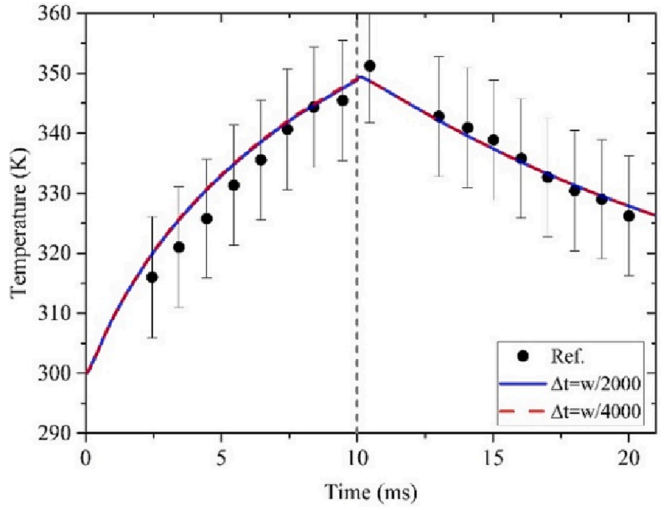

Fig. 3. Temporal evolution of temperature in CH_4/O_2/He mixture with 75% dilution at $\phi = 1$, $T_{in} = 300$ K, and $p = 60$ Torr assisted by 300 NSDs with $PRF = 30$ kHz and $E/N = 180$ Td.

temporal resolution-independent results, as can be seen in Fig. 3. The results show that the present numerical platform can well reproduce experimental data on plasma-assisted combustion.

4. Results and discussions

4.1. Effects of NSD and H_2 on ammonia combustion

Fig. 4 shows the IDT of ammonia/hydrogen/air as a function of X_{H2} and E_p, colored by the required preheat temperature (ΔT) to achieve the same level of enhancements in IDT without using NSD or hydrogen. It should be mentioned that 290 cases were simulated by varying X_{H2} and E_p values to obtain the results presented in Figs. 4–6, 10 and 11 by keeping the other plasma settings, including E/N, number of pulses, and PRF, constant. The ignition delay time of methane/air at an identical initial condition, i.e., $\phi = 1$, $T_{in} = 850$ K, and $p = 1$ atm, calculated by utilizing GRI-Mech 3.0 mechanism [62], is also shown for reference. The dashed line in Fig. 4 shows all the possible values of X_{H2} and E_p, using which the IDT of ammonia/air increases to the methane/air counterpart.

The results show that either only 1.7% of X_{H2} or 20 NSDs with $E_p =$

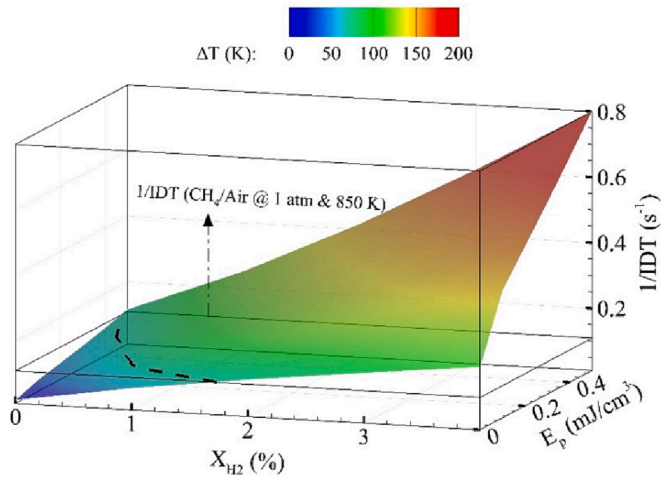

Fig. 4. Ignition delay time of ammonia mixtures as a function of X_{H2} and E_p for $\phi = 1$ and $p = 1$ atm colored by the required preheat temperature to achieve the same level of enhancements in ignition delay time without using NSD or hydrogen.

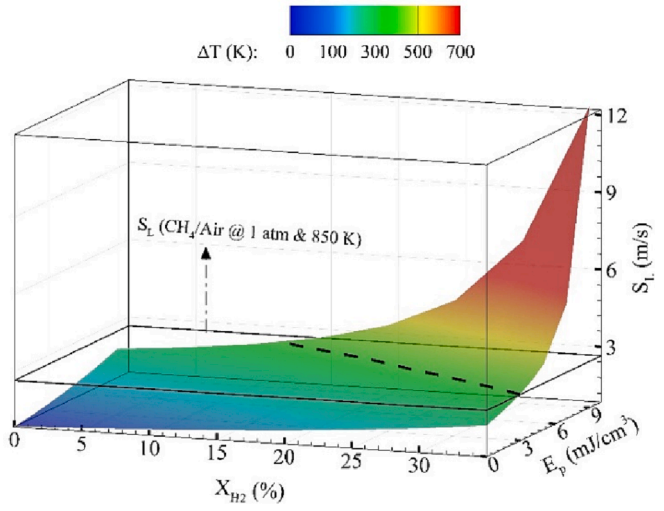

Fig. 5. Laminar flame speed of NH_3/H_2/air mixtures as a function of X_{H2} and E_p for $\phi = 1$ and $p = 1$ atm colored by the required preheat temperature to achieve the same level of enhancements in laminar flame speed without using NSD or hydrogen.

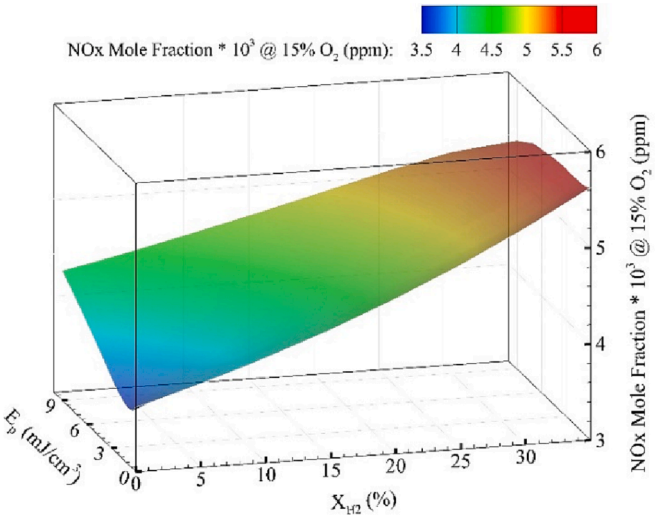

Fig. 6. NO_x emissions of NH_3/H_2/air flames as a function of X_{H2} and E_p for $\phi = 1$ and $p = 1$ atm.

0.45 mJ/cm^3 is needed to reduce the IDT of ammonia/air from 49.3 s to the methane/air counterpart, i.e., 9.6 s. The same enhancement in IDT is achievable by preheating the NH_3/air mixture by $\Delta T = 71$ K. To compare plasma-assisted combustion with preheating in terms of energy consumption, the required energy by each of these methods to reduce IDT of ammonia from 49.3 s to 9.6 s was calculated. It is found that plasma and preheating require 24 and 89 kJ/kg of the stoichiometric $NH_3/O_2/N_2$ mixture, respectively. This shows that using plasma is considerably cheaper than preheating the mixture to elevate the reactivity of ammonia. Fig. 4 also indicates that adding 4% hydrogen by volume to the fuel decreases the ignition delay time of ammonia by ten times, which is equivalent to preheating the NH_3/air mixture by $\Delta T = 146$ K. This result is in line with previously reported experimental data on the effects of hydrogen on ammonia ignition delay time [63,64]. Fig. 4 also shows that utilizing both plasma discharge and hydrogen simultaneously reduces the required X_{H2} or E_p to achieve a target IDT. For instance, discharging 20 NSDs with $E_p = 0.2$ mJ/cm^3 and $X_{H2} = 0.7\%$ is adequate to reduce the IDT of ammonia/air from 61.8 s to 9.6 s.

Contrary to IDT, considerably higher E_p and X_{H2} values are needed to

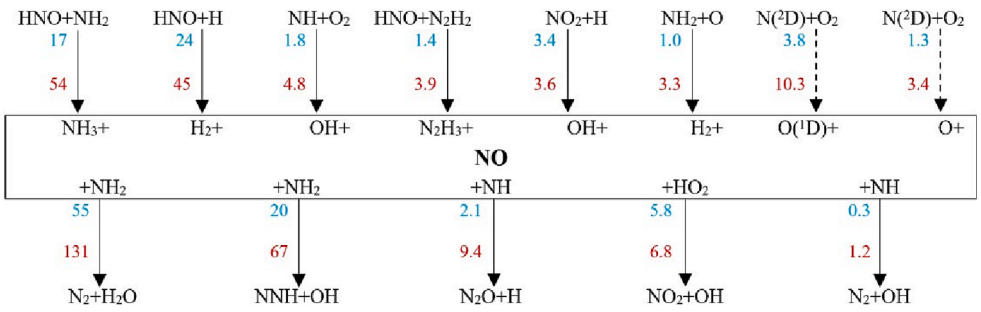

Fig. 7. Production and consumption rates (mol/m^{3}s) of NO during the plasma (dashed-arrows) and thermal (arrows) phases in plasma-assisted NH_3/H_2/air combustion with $E_p = 3$ mJ/cm^3 and $X_{H2} = 34.5\%$ (PAAC1-blue) and $E_p = 9$ mJ/cm^3 and $X_{H2} = 12\%$ (PAAC1-red) for $\phi = 1$ and $p = 1$ atm. (For interpretation of the references to colour in this figure legend, the reader is referred to the web version of this article.)

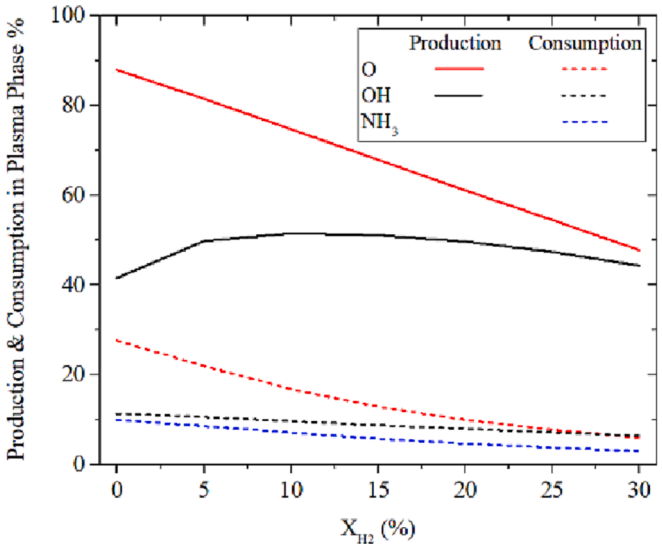

Fig. 8. Percentage of production and consumption of selected species during the plasma phase in NH_3/H_2/air mixtures as a function of X_{H2} for $\phi = 1$, $p = 1$ atm, and $E_p = 5$ mJ/cm^3.

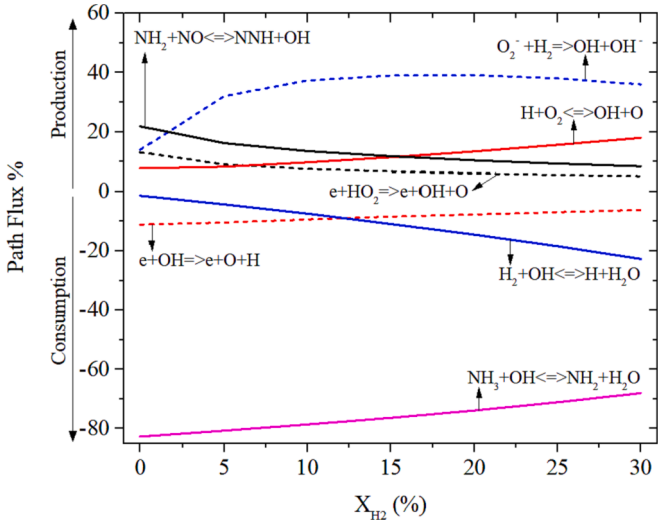

Fig. 9. Path flux of production and consumption of OH in plasma (dash lines) and thermal (lines) phases in NH_3/H_2/air mixtures as a function of X_{H2} for $\phi = 1$, $p = 1$ atm, and $E_p = 5$ mJ/cm^3.

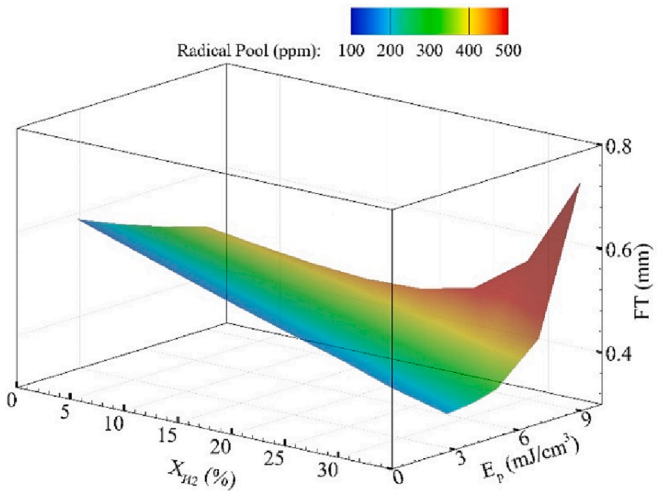

Fig. 10. Laminar flame thickness of NH_3/H_2/air colored by radical pool upstream of the flames as a function of X_{H2} and E_p for $\phi = 1$ and $p = 1$ atm.

noticeably increase the ammonia/air laminar flame speed. Fig. 5 shows the S_L of unstrained ammonia/hydrogen/air as a function of X_{H2} and E_p colored by the required preheat temperature to achieve the same level of enhancements in S_L without using NSD or hydrogen. The flame speed of methane/air at a similar initial condition is also shown for reference. The results show that even very high X_{H2} values, e.g., 35%, or 20 plasma pulses with $E_p = 11$ mJ/cm^3, are not solely enough to raise the ammonia/air flame speed to the methane/air counterpart. However, the dashed line drawn in Fig. 5 shows that combinations of plasma discharge and H_2 addition augment the S_L of ammonia to that of methane/air. Using 20 plasma pulses with $E_p = 9$ mJ/cm^3 and $X_{H2} = 12\%$ or $E_p = 7$ mJ/cm^3 and $X_{H2} = 21\%$ raises the S_L of ammonia/air from 0.88 m/s to 2.7 m/s, the methane/air flame speed. This enhancement can also be achieved by preheating the NH_3/air mixture by $\Delta T = 379$ K.

Despite the advantage of using the above methods to assist ammonia reactivity, NO_X emissions calculated downstream of the flame, plotted in Fig. 6, show that both high-energy NSDs and H_2 addition aggravate the level of NO_X emissions, being more pronounced at high X_{H2} values. Comparing the NO_X emissions in ammonia flames assisted by plasma and hydrogen to achieve the same level of enhancements in the flame speed, shown in Fig. 5, indicates that using plasma results in lower NO_X emissions than that in ammonia flames assisted by H_2. For instance, either using 20 NSDs with $E_p = 9$ mJ/cm^3 or $X_{H2} = 33.7\%$ raises ammonia flame speed from 0.88 m/s to 2 m/s. It can be found from Fig. 6 that NO_X emissions are 3675, 4350, and 5537 ppm in the pure ammonia flame without NSD, pure ammonia flame assisted by 20 NSDs with $E_p = 9$ mJ/cm^3, and a blend of ammonia and hydrogen flame with $X_{H2} = 33.7\%$, respectively. Accordingly, assisting the flame with NSDs

results in 27% lower NO_X emissions than the flame assisted by hydrogen for the above specific enhancement in the flame speed.

Here, two cases are compared to further evaluate the impacts of H_2 and NSDs on NO_X emissions of ammonia flames. In PAAC1, the flame is assisted more by H_2 rather than plasma, in which X_{H2} and E_p are 34.5% and 3 mJ/cm^3, respectively. In the second case (PAAC2), the mixture comprised 12% of H_2 assisted by plasma pulses with $E_p = 9$ mJ/cm^3. Both cases increase the flame speed of ammonia/air from 0.88 m/s to 2.7 m/s. Fig. 7 shows the rates of production (RoP) and consumption (RoC) of NO obtained over 20 plasma pulses for PAAC1 and PAAC2. In Fig. 7, reactions during the thermal and plasma phases are shown by arrows and dashed arrows, respectively. Here, the "thermal phase" denotes the simulation results between the pulses, while the "plasma phase" indicates the results over the pulse width. It can be noted that HNO plays a crucial role in NO formation in both cases. As expected, replacing NH_3 with H_2 encourages HNO to react with H rather than NH_2 to generate NO. Moreover, the plasma phase accounts for<10% of the total NO formation predominantly via, e.g., $N(^2D) + O_2 \rightarrow O(^1D) + NO$ chain branching reaction. In both cases, NO is consumed mostly in $NO + NH_2 \leftrightarrow N_2 + H_2O$ reaction. However, the RoC of NO via this reaction is higher in PAAC2 since the concentration of NH_2 is larger in PAAC2 than in PAAC1. Fig. 7 also indicates that both RoP and RoC of NO considerably increase by magnifying the contribution of the plasma discharge to assist combustion. The overall RoPs of NO are 0.057 and 0.138 kmol/m^{3}s for PAAC1 and PAAC2, while the RoCs of NO in the above cases are 0.084 and 0.217 kmol/m^{3}s, respectively. This shows that the RoP and RoC of NO increase, respectively, by a factor of 2.4 and 2.6 when PAAC1 is used instead of PAAC2. Therefore, the RoC of NO increases more than its RoP when the ammonia flame is assisted more by plasma discharge rather than H_2. This reveals why high-energy plasma discharges with low X_{H2} values have superior effects on ammonia combustion in terms of NO_X emissions as compared with low-energy plasma discharges with high X_{H2} values. Further investigations are needed to alleviate NO_X emissions in ammonia/hydrogen flames assisted by NSDs, e.g., using the staged combustion method [65,66].

To further analyze plasma-assisted ammonia oxidation in the presence of H_2, the percentage of production and consumption fluxes of the key radicals and species controlling ammonia oxidation are plotted in Fig. 8 for different X_{H2} values. The fluxes were obtained over 20 NSDs with $E_p = 5$ mJ/cm^3. Here, for the sake of brevity, only the details of the reaction path fluxes of OH are shown in Fig. 9, while conspicuous details of path flux analyses of other species are summarized as follows. Fig. 8 shows that increasing X_{H2} reduces the plasma contribution in cracking the fuel. In the pure ammonia case, $NH_3 + OH \leftrightarrow NH_2 + H_2O$, $O(^1D) + NH_3 \rightarrow OH + NH_2$, and $NH_3 + O \leftrightarrow NH_2 + H_2O$ reactions are responsible for 81.6%, 6.5%, and 4.5% dissociation of the fuel, respectively. However, for instance, for $X_{H2} = 30\%$, $NH_3 + OH \leftrightarrow NH_2 + H_2O$ and $NH_3 + O \leftrightarrow NH_2 + H_2O$ dissociate 87% and 10% of the fuel, while $O(^1D) + NH_3 \rightarrow OH + NH_2$ reaction contributes by<2% in NH_3 dissociation. As one of the key radicals for NH_3 dissociation, O in pure ammonia case is mainly produced during the plasma phase via $O_2^- + H \rightarrow OH^- + O$, $e + HO_2 \rightarrow e + O + H$, $e + OH \rightarrow e + O + H$ reactions with 33.6%, 19.7%, and 12.6% contributions, respectively, while 12% of O originates from the thermal phase, i.e., from $H + O_2 \leftrightarrow OH + O$ reaction. Adding H_2 to the fuel increases the impact of the thermal phase in producing O, as shown in Fig. 8, e.g., 50.4% of O routes from $H + O_2 \leftrightarrow OH + O$ when X_{H2} is 30%.

Fig. 8 shows that both plasma and thermal phases account for almost an identical amount of OH production, the other key radical in NH_3 dissociation. The percentage contribution of plasma in generating OH is less dependent on X_{H2} than that in generating O radical. Furthermore, Fig. 8 shows that the contribution of the plasma phase in producing OH changes non-monotonically with X_{H2}. This radical in the pure ammonia case is predominantly produced via $NH_2 + NO \leftrightarrow NNH + OH$ reaction, as shown in Fig. 9. The contribution of this reaction in OH production is overtaken by $O_2^- + H_2 \rightarrow OH + OH^-$ and $H + O_2 \leftrightarrow OH + O$ reactions when the X_{H2} is>2% and 15%, respectively. This can be a manifestation of shifting ammonia oxidation pathways from N-species reactions to the H_2/O_2 system as the X_{H2} increases. Fig. 9 shows that although OH production via $e + HO_2 \rightarrow e + OH + O$ drops by raising X_{H2}, $O_2^- + H_2 \rightarrow OH + OH^-$ generates more OH radicals at high X_{H2} values than that at low X_{H2}. This indicates why the contribution of plasma in OH production changes non-monotonically by altering X_{H2}. The results also show that NH_3 and H_2 compete for OH, which is in line with previous studies on NH_3/H_2 oxidation [10,67]. The key reactions consuming OH, shown in Fig. 9, respond almost linearly to changes in X_{H2}. The slope of the linear curves fitted to OH consumption via $H_2 + OH \leftrightarrow H + H_2O$, $NH_3 + OH \leftrightarrow NH_2 + H_2O$, and $e + OH \rightarrow e + O + H$ reactions as functions of X_{H2} for $0 < X_{H2} < 30\%$ are −0.7, 0.5, 0.2, respectively. This shows that H_2 competes more with NH_3 than $e + OH \rightarrow e + O + H$ electron impact reaction for OH.

Abrupt changes in the flame speed observed in Fig. 5 would be a symptom of manipulations in the flame's inner structure, as reported in our previous study on pure ammonia flames assisted by NSDs [41]. Fig. 10 shows the unstrained flame thickness of $NH_3/H_2/O_2/N_2$ assisted by NSDs. The flame thickness is defined as $(T_b–T_u)/(dT/dX)_{Max}$, where T_b is the temperature of the burnt gases, T_u is the mixture temperature at the end of the constant-pressure reactor, and $(dT/dX)_{Max}$ is the maximum temperature gradient through the flame [68]. The result is colored by the radical pool comprising O, OH, H, and HO_2 recorded at the inlet of the reactor used to model the one-dimensional freely-propagating flame, i.e., at the end of 20 plasma pulses discharged in the adiabatic constant-pressure reactor.

The results show that unstrained flame thickness decreases either by using NSDs with $E_p < 10$ mJ/cm^3 or by adding H_2 to the mixture. Intriguingly, using NSDs with $4.1 < E_p < 6.8$ mJ/cm^3 in NH_3/H_2 blends with high X_{H2} values, e.g., $22 < X_{H2} < 35\%$, thickens the flame structure. Similar thickenings were observed in our previous investigations for ammonia/air flames assisted by NSDs with considerably higher pulse energy density values, i.e., $E_p > 20$ mJ/cm^3 [41]. Interestingly, Fig. 10 reveals that adding H_2 to the fuel expedites the thickening process by lowering the required pulse energy density values to establish the thickened flame. At low E_p values, regardless of the X_{H2}, there is a negligible radical pool upstream of the flame. However, the concentration of radicals dramatically rises when both E_p and the X_{H2} values are increased simultaneously. This shows that the flame-thickening process is highly dependent on the radical pool generated by the plasma discharges, which boosts the chemical reactions on the low-temperature side of the flame, broadening the reaction zone.

Besides the unstrained flame characteristics, it is important to eval-

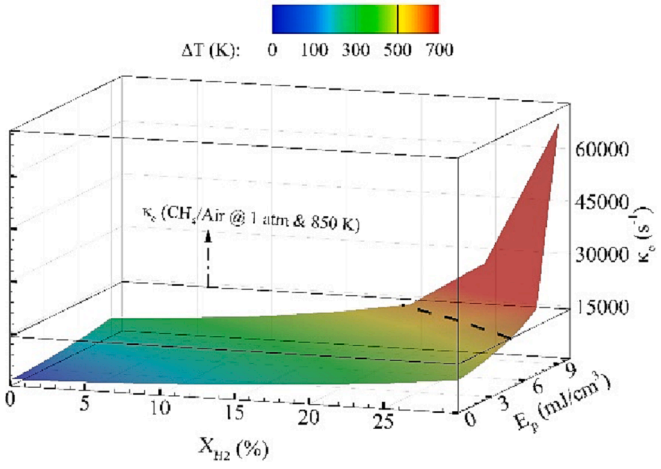

Fig. 11. Extinction strain rate of NH_3/H_2/air flames as a function of X_{H2} and E_p for $\phi = 1$ and $p = 1$ atm colored by the required preheat temperature to achieve the same level of enhancement in extinction strain rate without using NSD or hydrogen.

uate the effects of NSDs on strained flame features. Fig. 11 shows the extinction strain rate (κ_e) of plasma-assisted NH_3/H_2/air flames. The extinction strain rate of CH_4/air flame at a similar thermodynamic condition is shown in Fig. 11 for reference. The dashed line shows the required E_p and X_{H2} values to raise the extinction strain rate of ammonia to its methane counterpart. The results show that using 24.8% of H_2 in the fuel alongside NSD with $E_p = 7$ mJ/cm^3 raises the extinction strain rate of ammonia/air from 1888 s^{-1} to 14200 s^{-1}, the extinction strain rate of CH_4/air. The same enhancements in κ_e are achievable by pre-heating the NH_3/air mixture by $\Delta T = 585$ K. To compare the response of ammonia flames assisted by plasma with those aided by hydrogen to strain, consumption speeds of four flames are plotted in Fig. 12 as functions of the imposed strains. The extinction strain rates of cases with $E_p = 3$ mJ/cm^3 & $X_{H2} = 0\%$ and $E_p = 0$ mJ/ cm^3 & $X_{H2} = 6.6\%$ are 2530 s^{-1}, while those for $E_p = 7$ mJ/cm^3 & $X_{H2} = 0\%$ and $E_p = 0$ mJ/cm^3 & $X_{H2} = 17\%$ are 4190 s^{-1}. Linear curves are fitted to the numerical data, and the corresponding slopes are presented in the legend in Fig. 12 to properly compare different cases. It should be noted that the effective Lewis numbers of the selected cases calculated by using the method proposed by Bechtold and Matalon are in the range of 0.96–0.98 [69], which indicates that the selected conditions have nearly the same differential diffusion of heat and mass. Here, the consumption speed is calculated below,

$$CS = \frac{\int_{-L/2}^{L/2} \frac{HRR}{C_p} dx}{\rho_u (T_b - T_u)} \quad (2)$$

where L is the length of the computational domain between two burners, HHR is the volumetric heat release rate, C_p heat capacity at constant pressure, T_b is the temperature of burnt gases, and ρ_u and T_u are the mixture density and temperature at the end of the constant-pressure reactor, respectively.

In Fig. 12, consumption speeds and strain rates are normalized by the corresponding values at the extinction state. The results show that the magnitudes of the slopes are lower when the flame is assisted by plasma rather than by H_2, which shows that the consumption speed is less prone to the strain rate value in plasma-assisted ammonia flames than that in ammonia flames assisted by hydrogen for a given enhancement in the extinction strain rate. This is because the heat transfer from the reaction zone to the preheat zone is fast at a high strain rate. When the strain rate is high enough, e.g., above the extinction strain rate, the heat loss from the reaction zone is faster than the heat release in the reaction zone, and as a result, the reactions in the flame are quenched. In plasma-assisted flames, the production of radicals is boosted by plasma discharge, which is not sensitive to local temperature and heat loss from the reaction zone.

4.2. Effects of equivalence ratio on plasma-assisted NH_3/H_2/air combustion

Fig. 13 shows NO_X emissions from ammonia flames with different equivalence ratios assisted by plasma pulses and hydrogen. NO_X emissions in most cases increase monotonically with E_p and X_{H2} for the present selected plasma settings. Interestingly, the combination of high-energy NSDs, i.e., with $E_p > 6$ mJ/cm^3, and high H_2 fuel fractions, e.g., $X_{H2} = 30\%$, reduces NO_X emissions of lean ammonia flames. This can be a manifestation of the $DeNO_X$ process. To address this, the NO_X emissions through the flames assisted by NSDs are plotted in Fig. 14. In high-energy plasma cases, NO_X levels are considerably high in the preheating zone. Nevertheless, a portion of this NO_X is consumed in the flame preheating zone, shown by $DeNO_{X1}$ in Fig. 14. The results show that NO_X is also consumed in the post-flames, $DeNO_{X2}$ in Fig. 14, being more noticeable under low-energy plasma discharges for the rich mixture. This is in line with previous investigations by Shmakov *et al.* in which they showed that $DeNO_X$ is more intense in the post-flame of rich $H_2/O_2/N_2/NO/NH_3$ mixtures than that for lean mixtures [70]. It can be found from Fig. 14 that $DeNO_{X1}$ results in 382 and 271 ppm reduction in NO_X in lean and rich mixtures assisted by plasma discharges with $E_p = 9$ mJ/cm^3, while 90 and 80 ppm of NO_X are consumed by $DeNO_{X2}$ in the lean and rich cases assisted by high-energy plasma discharges, respectively. This shows that both $DeNO_{X1}$ and $DeNO_{X2}$ are more intense in the lean mixture than those in the rich flame assisted by high-energy plasma pulses. This reveals why NO_X emissions drop by discharging high-energy pulses in lean NH_3/H_2/air flames with $X_{H2} = 30\%$, observed in Fig. 13. It should be mentioned that for all the mixtures, there is a certain value of E_p beyond which further increases in E_p decrease NO_X emissions. For instance, our previous investigations showed that NO_X emissions of NH_3/air flames with $\phi = 0.8$ initially at $T_{in} = 850$ K and $p = 1$ atm drop if $E_p > 16$ mJ/cm^3 [41], while Fig. 13 shows that a lower E_p, i.e., 6 mJ/cm^3, is needed to reduce NO_X in lean NH_3/H_2/air flames.

Further analyses were carried out to find the key mechanisms controlling $DeNO_X$ processes in ammonia/hydrogen flames assisted by plasma. Fig. 15 shows the RoP and RoC of NO in NH_3/H_2/air flames with $X_{H2} = 15\%$ and $\phi = 0.8$ and 1.2 assisted by plasma discharges with $E_p =$ 0.1 and 9 mJ/cm^3. The rates were obtained over 20 plasma pulses. The

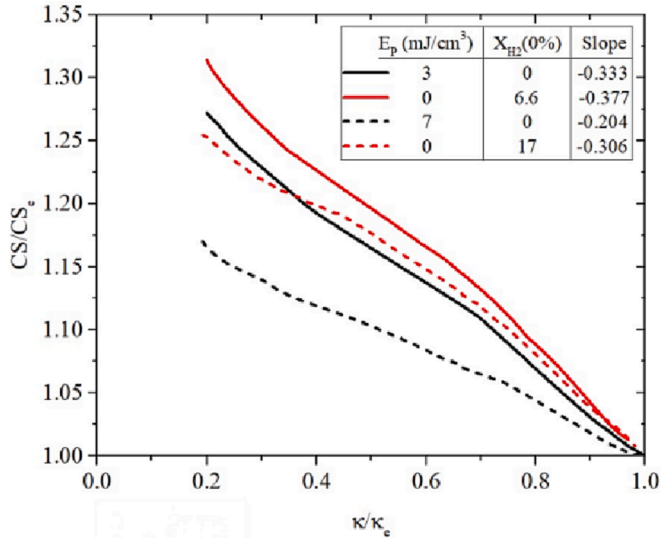

Fig. 12. Normalized consumption speed as a function of normalized strain rate for NH_3/H_2/air flames at $\phi = 1$ and $p = 1$ atm.

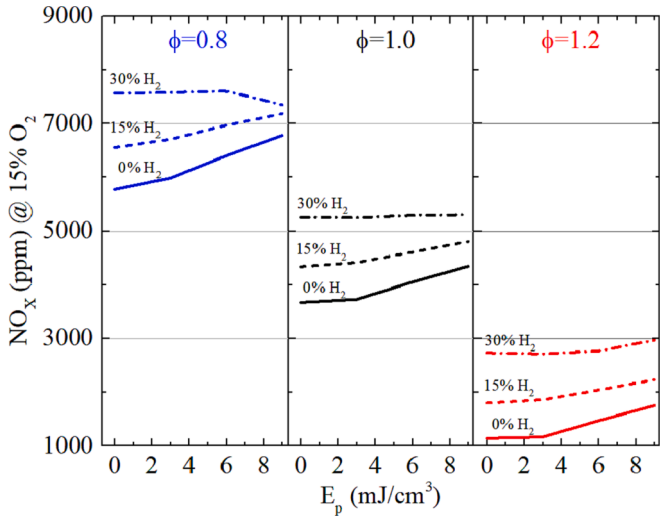

Fig. 13. NO_X emissions of different flames as a function of X_{H2}, E_p, and ϕ for $p = 1$ atm.

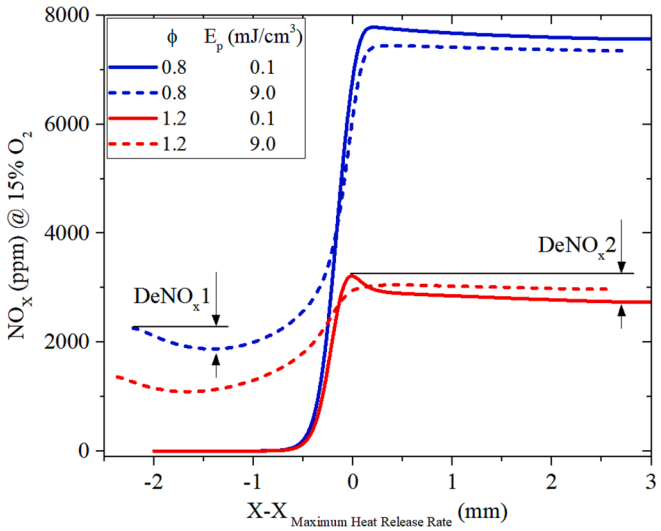

Fig. 14. NO_X emissions through plasma-assisted NH_3/H_2/air flames with X_{H2} = 15%, ϕ = 0.8 and 1.2, E_p = 0.1 and 9 mJ/cm^3 for p = 1 atm.

results show that the RoP and RoC of NO are slightly higher in the rich mixture than those in the lean case when the mixtures are stimulated by a low pulse energy density value. In such a condition, the overall RoP of NO is higher than the RoC in both lean and rich mixtures. The overall RoP and RoC of NO are 0.29 and −0.22 kmol/m^{3}s in the lean mixture assisted by plasma with E_p = 0.1 mJ/cm^3, while those in the rich mixture stimulated by plasma with E_p = 0.1 mJ/cm^3 are 0.31 and −0.24 kmol/m^{3}s, respectively. Contrary to this, in high-energy plasma cases, the overall RoC of NO is higher than its RoP, which is a clear manifestation of the $DeNO_X$ mechanism. It can be found from Fig. 15 that the rates are noticeably higher in the lean mixture than the corresponding values in the rich mixture. The RoCs of NO are −0.39 and −0.32 kmol/m^{3}s in the lean and rich mixtures assisted by plasma with E_p = 9 mJ/cm^3. This shows why $DeNO_X$ is more intense in the lean mixture than in the rich case.

Fig. 15 also shows that $HNO + NH_2 \leftrightarrow NH_3 + NO$ is the main source of NO in low-energy plasma cases. Nevertheless, as the pulse energy density increases $HNO + H \leftrightarrow NO + H_2$ overtakes $HNO + NH_2 \leftrightarrow NH_3 + NO$ in producing NO, since the higher E_p, the faster fuel dissociation down to H radical. This shows that NO is produced through fuel chemistry rather than thermal NO pathways, e.g., $N_2 + O \leftrightarrow N + NO$ and $N + O_2 \leftrightarrow NO + O$, which is in agreement with previous studies on NH_3/H_2/Air flames [20]. In all the selected cases, NO mainly reacts with NH_2 to generate H_2O and N_2. However, a considerable amount of NO reacts with NH_2 in high pulse energy density cases to produce OH radicals, which subsequently boost the chemical reactions to further dissociate the fuel.

Fig. 16 shows the unstrained flame thickness for different equivalence ratios as a function of E_p and X_{H2}. The results reveal that the selected pulse energy density values are not adequate to thicken the pure ammonia flames. Interestingly, lower E_p values are needed to broaden the reaction zone of the rich NH_3/H_2/air flames than those required by the lean and stoichiometric mixtures. For instance, the rich flame with X_{H2} = 30 % is thickened by discharging plasma with low E_p values, e.g., E_p = 1 mJ/cm^3, while plasma pulses with E_p = 3 mJ/cm^3 are needed to broaden the reaction zones in lean and stoichiometric mixtures with X_{H2} = 30 %.

In order to find an explanation for the above observation, the temperature and radical pools upstream of the one-dimensional premixed flames with X_{H2} = 15% are plotted in Fig. 17 as functions of E_p. As expected, the lean mixture assisted by 20 pulses of plasma contains slightly higher O radicals, especially when the pulse energy density is higher than 6 mJ/cm^3. This is due to the abundant concentration of O_2 in lean mixtures. On the other hand, compared to the lean and stoichiometric mixtures, H concentration is considerably higher in the rich mixture even for very low E_p values, e.g., 1 mJ/cm^3. However, the OH radical is almost independent of the equivalence ratio for a given E_p. It is interesting to note that the temperature is slightly higher in the lean mixture than those in the rich and stoichiometric cases for a given E_p, which indicates that the thickening process is a non-thermal process and is directly controlled by the radical pool, especially by H. It should be mentioned that further details of the effects of equivalence ratio on IDT, S_L, and κ_e of ammonia/air flames for various E_p and X_{H2} values are presented in the Supplementary Materials (Figs. S2–S4). The range of E_p and X_{H2} were selected based on the analyses presented in section 4.1 to properly assist ammonia flames.

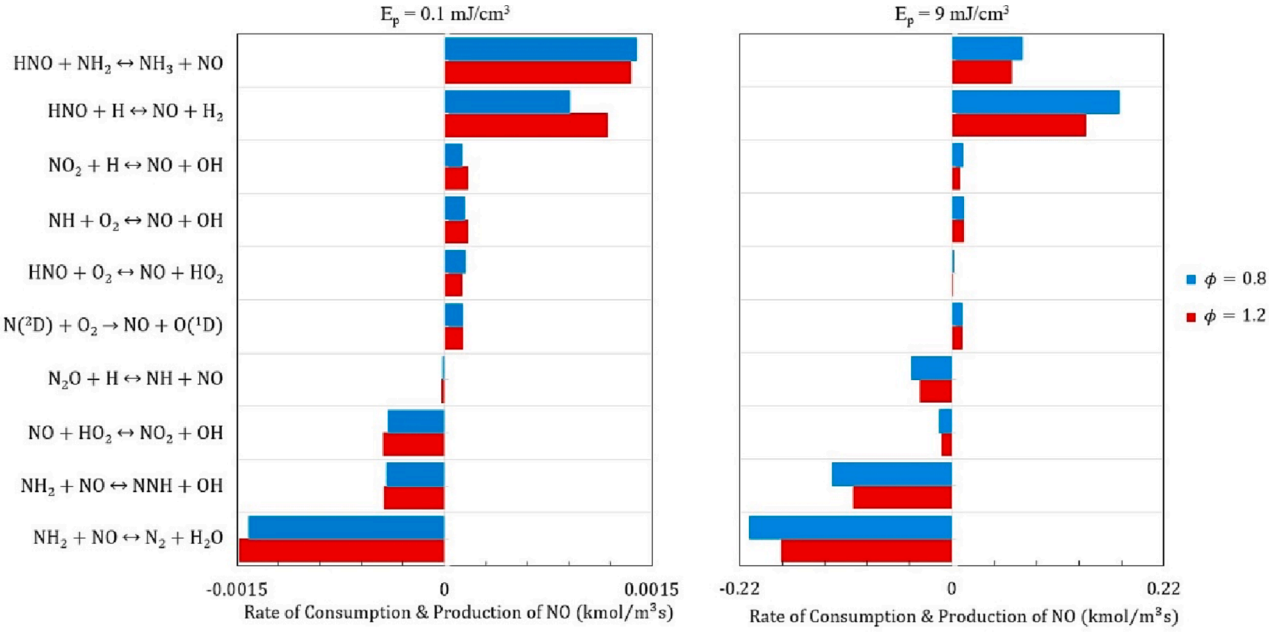

Fig. 15. Rate of consumption and production of NO in plasma-assisted NH_3/H_2/air mixtures with X_{H2} = 15%, ϕ = 0.8 and 1.2, E_p = 0.1 and 9 mJ/cm^3 for p = 1 atm.

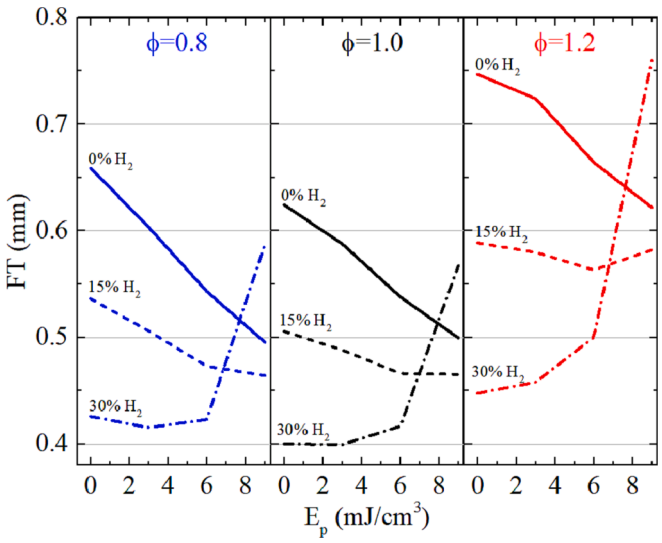

Fig. 16. Flame thickness as a function of X_{H2}, ϕ, and E_p for $p = 1$ atm.

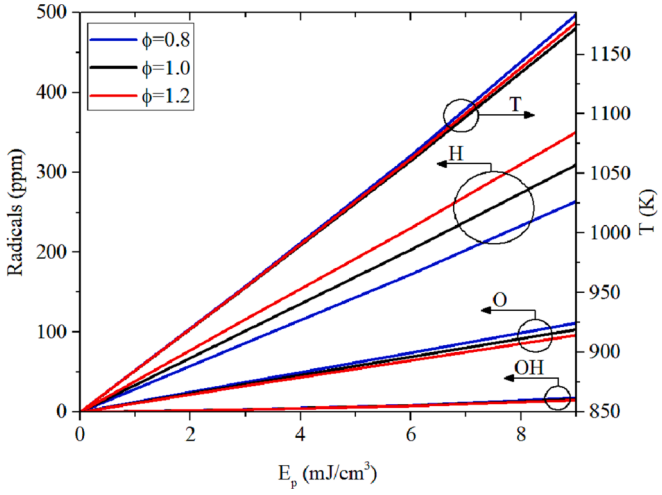

Fig. 17. Radicals and temperature upstream of NH_3/H_2/air flames with $X_{H2} =$ 15% as functions of ϕ and E_p for $p = 1$ atm.

4.3. Effects of pressure on plasma-assisted NH_3/H_2/air combustion

Previous investigations by Wolk *et al.* on methane/air ignition by utilizing microwave spark plugs showed that increasing the mixture pressure abates the impacts of microwave on the ignition, believed to be due to the decreases in E/N [71]. Increasing the mixture pressure raises the number density of neutrals, which in turn reduces E/N for a given plasma setting, i.e., E. However, our previous study showed that characteristics of ammonia combustion are non-monotonically dependent on changes in E/N [41]. The questions posed here are, "how do characteristics of plasma-assisted ammonia combustion change by pressurizing the mixture?" and "how are such changes related to E/N variations caused by changing the mixture pressure?". To properly answer these questions, two sets of simulations were performed, namely by keeping (1) E and (2) E/N constant. In the first strategy, in each case, E is kept constant, which is calculated by multiplying the reduced electric field, i.e., 350 Td, by the number density of neutrals in the fresh reactants in atmospheric cases. This strategy results in a proportional reduction of E/N with pressure augmentations. In the latter strategy, E increases by raising the mixture pressure since the higher p, the more N, and correspondingly the higher E needed to keep E/N constant. It should be mentioned that both strategies result in a unique solution under atmospheric conditions for a given mixture composition.

Fig. 18 shows the IDT of a selected number of cases with different E_p, X_{H2}, and p values. Here, lines show the results obtained by keeping the E/N constant, while lines with symbols indicate the numerical results in which E was kept constant. The results show that increasing the mixture pressure weakens the impacts of plasma and H_2 in reducing the IDT of ammonia, being more pronounced for plasma effects. For instance, IDT of the non-plasma ammonia/air case, i.e., $E_p = 0$ mJ/cm^3, drops by 90% at $p = 1$ atm by injecting 4% H_2 in the fuel, while the corresponding reduction in IDT at $p = 5$ atm is 75%. Moreover, discharging 20 pulses with a fixed E and $E_p = 0.5$ mJ/cm^3 reduces the IDT of the non-plasma ammonia/air mixture by 83% and 45% at $p = 1$ and 5 atm, respectively. The corresponding reduction in IDT by keeping E/N constant is 66% for $p = 5$ atm. This shows that, as expected, the impacts of plasma on IDT intensify by increasing the electric field. However, adding to E proportionally with pressure augmentations does not lead to an identical flame enhancement as that under atmospheric conditions. Therefore, it can be concluded that E/N is not the only controlling parameter depleting the plasma effects on ammonia ignition delay time under pressurized conditions.

Laminar flame speed plotted in Fig. 19, as well as the extinction strain rate, flame thickness, and NO_X emissions presented in Supplementary Materials (Figs. S5–S7, respectively) as functions of X_{H2}, E_p, and p support the above conclusions by showing that pressure significantly reduces plasma effects on the characteristics of a one-dimensional premixed flame. Furthermore, E/N plays a negligible role in suppressing plasma impacts on the flame characteristics at high-pressure values.

To elaborate on the impacts of pressure on plasma-assisted combustion, path flux analyses were carried out for four cases by varying the p and E_p in the ranges of 1–5 atm and 1–9 mJ/cm^3, respectively. The other plasma settings, e.g., E, and mixture specifications, were kept constant, including X_{H2}, which is set at 15% in all cases. The fluxes were obtained over 20 NSDs. The path fluxes of NH_3, presented in Supplementary Material (Fig. S8), show that ammonia is mainly dissociated by OH to generate NH_2 and H_2O in all the selected cases, while $O(^1D) + NH_3 \rightarrow NH_2 + OH$ contributes to dissociating ammonia by<4%. The path fluxes of OH, as the key radical to dissociate NH_3, plotted in Fig. 20, show that $O_2^- + H_2 \rightarrow OH^- + OH$ charge exchange and $H + O_2 \leftrightarrow O + OH$ chain branching reactions are the main pathways to generate OH under atmospheric conditions for $E_p = 9$ mJ/cm^3. Increasing the mixture pressure shifts the OH production path to $NH_2 + HO_2 \leftrightarrow H_2NO + OH$ and

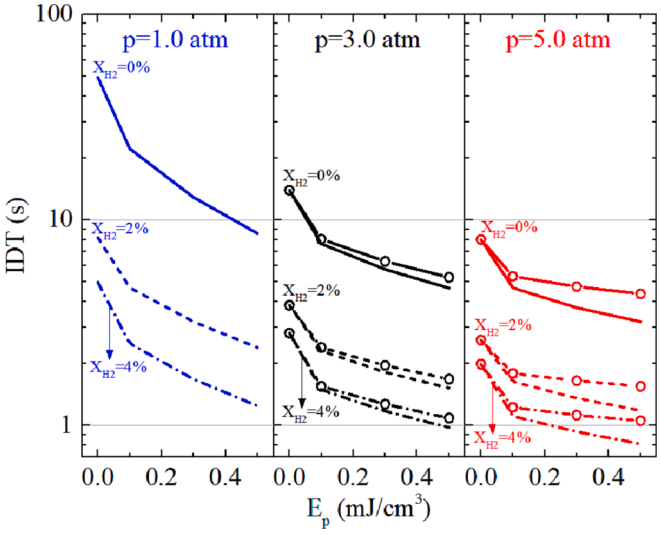

Fig. 18. Ignition delay time of ammonia as a function of E_p, X_{H2}, and p for $\phi =$ 1. Lines with symbols show simulation results in which E was kept constant, and lines show the results obtained by keeping E/N constant at 350 Td.

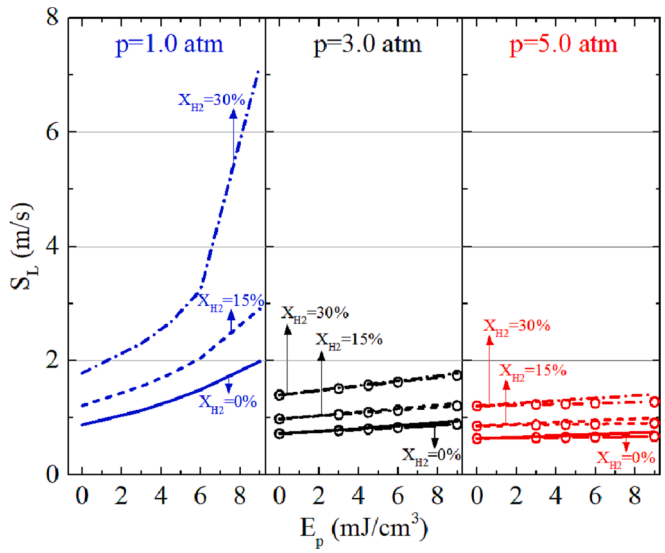

Fig. 19. Laminar flame speed of ammonia as a function of E_p, X_{H2}, and p for $\phi = 1$. Lines with symbols show simulation results in which E was kept constant, and lines show the results obtained by keeping E/N constant at 350 Td.

NO + HO_2 ↔ NO_2 + OH reactions, which shows the importance of the HO_2 radical in OH production. The path fluxes of HO_2 plotted in Fig. 20 show that increasing the mixture pressure substantially activates the third body reaction H + O_2 + M ↔ HO_2 + M in producing HO_2. However, increasing E_p slightly reduces such impacts by activating other paths to generate HO_2 radicals, e.g., N_2H_3 + O_2 ↔ N_2H_2 + HO_2. This shows that plasma impacts on combustion at high-pressure conditions are suppressed by pressure-dependent reactions.

5. Conclusions

Numerical simulations were performed to study the synergetic effects of nanosecond plasma discharge and hydrogen on ammonia combustion. To this end, a new kinetic model was assembled comprising the excitations, ionizations, quenching, recombination, charge exchanges, and neutral state elementary reactions for $NH_3/H_2/O_2/N_2$ mixtures. The multi-time-scale chemical reactions during plasma and thermal phases were resolved by utilizing a non-uniform time-step method. The numerical model was used to investigate the impacts of plasma and hydrogen addition on the combustion and emission characteristics of ammonia flames.

The results showed that relatively low energy pulses or low hydrogen fuel fractions are enough to noticeably reduce the ignition delay time of ammonia/air. However, even very high-energy pulses, e.g., 20 pulses with an energy density of 11 mJ/cm^3 or high amount of hydrogen addition, e.g., 30% hydrogen by volume in the fuel, are insufficient to raise the flame speed or extinction strain rate of ammonia to those of widely used fuels, e.g., methane. Such enhancements can be achieved by using plasma and hydrogen together, both at moderate levels, e.g., plasma with E_p = 9 mJ/cm^3 and X_{H2} = 12%. It was shown that for a specific enhancement in the flame speed, assisting an ammonia/air flame by NSDs results in less NO_X emissions than those assisted by H_2. Furthermore, plasma increases the resilience of the flame to the strain. The reduction of NO_X emissions is due to the $DeNO_X$ mechanisms both at preheating and post-flame zones, which are more pronounced under lean conditions than in the rich and stoichiometric cases. The present study showed that discharging high-energy pulses can thicken reaction zones by generating radical pools upstream of the flame. The required pulse energy density to trigger such manipulations in the flame inner structure drops by increasing the hydrogen fuel fraction. The simulation results revealed that pressurizing the mixture conspicuously deteriorates the plasma effects on combustion. Increasing the electric field linearly with pressure cannot compensate for the suppressing effects of pressure on the plasma discharges. It appears that the effects of pressure on plasma-assisted combustion are not predominantly due to changes in the reduced electric field caused by raising the mixture's pressure.

CRediT authorship contribution statement

Mohammad Shahsavari: Conceptualization, Methodology, Software, Validation, Formal analysis, Investigation, Writing – original draft, Writing – review & editing. **Alexander A. Konnov:**

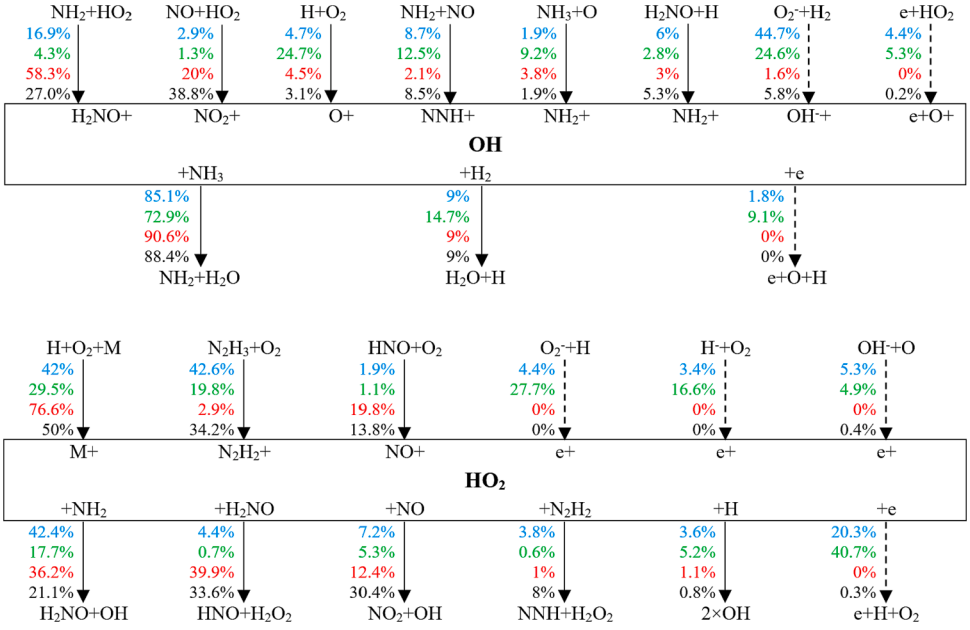

Fig. 20. Path fluxes of OH (top) and HO_2 (bottom) during the plasma (dashed arrows) and thermal (arrows) phases in plasma-assisted NH_3/H_2/air combustion with X_{H2} = 15%, ϕ = 1, fixed E, and E_p = 1 mJ/cm^3 and p = 1 atm (blue), E_p = 9 mJ/cm^3 and p = 1 atm (green), E_p = 1 mJ/cm^3 and p = 5 atm (red), and E_p = 9 mJ/cm^3 and p = 5 atm (black). (For interpretation of the references to colour in this figure legend, the reader is referred to the web version of this article.)

Conceptualization, Writing – review & editing. **Xue-Song Bai:** Writing – review & editing. **Agustin Valera-Medina:** Conceptualization, Writing – review & editing. **Tie Li:** Writing – review & editing. **Mehdi Jangi:** Conceptualization, Supervision, Methodology, Writing – review & editing.

Declaration of Competing Interest

The authors declare that they have no known competing financial interests or personal relationships that could have appeared to influence the work reported in this paper.

Data availability

Data will be made available on request.

Acknowledgements

This study, as a part of PlasNH3 project, was supported by Marie Sklodowska-curie Foundation through MSCA-IF-EF-ST action, H2020-MSCA-IF-2020 call. AAK and XSB grateful to the Knut and Alice Wallenberg Foundation for the financial support through grant KAW2019.0084 COCALD. Cardiff University gratefully acknowledges the support from the Welsh European Funding Office through "Flexible Integrated Energy Systems", project 80835.

Appendix A. Supplementary data

Supplementary data to this article can be found online at https://doi.org/10.1016/j.fuel.2023.128475.

References

[1] Kobayashi H, Hayakawa A, Kunkuma K, Somarathne A, Okafor E. Science and technology of ammonia combustion. Proc Combust Inst 2019;37:109–33.
[2] Valera-Medina A, Amer-Hatem F, Azad A, Dedoussi I, de Joannon M, Fernandes R, et al. Review on Ammonia as a Potential Fuel: From Synthesis to Economics. Energy Fuels 2021;35:6964–7029.
[3] Okafor E, Somarathne K, Ratthanan R, Hayakawa A, Kudo T, Kurata O, et al. Control of NOx and other emissions in micro gas turbine combustors fuelled with mixtures of methane and ammonia. Combust Flame 2020;211:406–16.
[4] Colson S, Kuhni M, Hayakawa A, Kobayashi H, Galizzi C, Escudié D. Stabilization mechanisms of an ammonia/methane non-premixed jet flame up to liftoff. Combust Flame 2021;234. https://doi.org/10.1016/j.combustflame.2021.111657.
[5] Zhang X, Moosakutty S, Rajan R, Younes M, Sarathy S. Combustion chemistry of ammonia/hydrogen mixtures: Jet-stirred reactor measurements and comprehensive kinetic modeling. Combust Flame 2021;234. https://doi.org/10.1016/j.combustflame.2021.111653.
[6] Chen P, Fang Y, Wang P, Gu M, Luo K, Fan J. The effect of ammonia co-firing on NO heterogeneous reduction in the high-temperature reduction zone of coal air-staging combustion: Experimental and quantum chemistry study. Combust Flame 2022;237. https://doi.org/10.1016/j.combustflame.2021.111857.
[7] Zhou S, Yang W, Tan H, An Q, Wang J, Dai H, et al. Experimental and kinetic modeling study on NH3/syngas/air and NH3/bio-syngas/air premixed laminar flames at elevated temperature. Combust Flame 2021;233. https://doi.org/10.1016/j.combustflame.2021.111594.
[8] Issayev G, Giri B, Elbaz A, Shrestha K, Mauss F, Roberts W, et al. Combustion behavior of ammonia blended with diethyl ether. Proc Combust Inst 2021;38:499–506.
[9] Zhang M, Wei X, Wang J, Huang Z, Tan H. The blow-off and transient characteristics of co-firing ammonia/methane fuels in a swirl combustor. Proc Combust Inst 2021;38:5181–90.
[10] Gotama G, Hayakawa A, Okafor E, Kanoshima R, Hayashi M, Kudo T, et al. Measurement of the laminar burning velocity and kinetics study of the importance of the hydrogen recovery mechanism of ammonia/hydrogen/air premixed flames. Combust Flame 2022;236. https://doi.org/10.1016/j.combustflame.2021.111753.
[11] Wiseman S, Rieth M, Gruber A, Dawson J, Chen J. A comparison of the blow-out behavior of turbulent premixed ammonia/hydrogen/nitrogen-air and methane–air flames. Proc Combust Inst 2021;38:2869–76.
[12] Valera-Medina A, Pugh D, Marsh P, Bulat G, Bowen P. Preliminary study on lean premixed combustion of ammonia-hydrogen for swirling gas turbine combustors. Int J Hydrog Energy 2017;42:24495–503.
[13] Zhu X, Khateeb A, Guiberti T, Roberts W. NO and OH* emission characteristics of very-lean to stoichiometric ammonia–hydrogen–air swirl flames. Proc Combust Inst 2021;38:5155–62.
[14] Franco M, Rocha R, Costa M, Yehia M. Characteristics of NH3/H2/air flames in a combustor fired by a swirl and bluff-body stabilized burner. Proc Combust Inst 2021;38:5129–38.
[15] Sun Y, Cai T, Shahsavari M, Sun D, Sun X, Zhao D, et al. RANS simulations of combustion and emission characteristics of a premixed NH3/H2 swirling flame with reduced chemical kinetic model. Chinese J Aeronaut 2021;34:17–27.
[16] Cai T, Zhao D, Chan SH, Shahsavari M. Tailoring reduced mechanisms for predicting flame propagation and ignition characteristics in ammonia and ammonia/hydrogen mixtures. Energy 2022;260. https://doi.org/10.1016/j.energy.2022.125090.
[17] Zhao H, Zhao D, Becker S, Zhang Y. NO emission and enhanced thermal performances studies on counter-flow double-channel hydrogen/ammonia-fuelled mixrocombustors with oval-shaped internal threads. Fuel 2023;341. https://doi.org/10.1016/j.fuel.2023.127665.
[18] Glarborg P, Miller J, Ruscic B, Klippenstein S. Modeling nitrogen chemistry in combustion. Prog Energy Combust Sci 2018;67:31–68.
[19] Valera-Medina A, Xiao H, Owen-Jones M, David W, Bowen P. Ammonia for power. Prog Energy Combust Sci 2018;69:63–102.
[20] Netzer C, Ahmed A, Gruber A, Løvås T. Curvature effects on NO formation in wrinkled laminar ammonia/hydrogen/nitrogen-air premixed flames. Combust Flame 2021;232. https://doi.org/10.1016/j.combustflame.2021.111520.
[21] Goldmann A, Dinkelacker F. Investigation of boundary layer flashback for non-swirling premixed hydrogen/ammonia/nitrogen/oxygen/air flames. Combust Flame 2022;238. https://doi.org/10.1016/j.combustflame.2021.111927.
[22] Kurata O, Iki N, Matsunuma T, Inoue T, Tsujimura T, Furutani H, et al. Performances and emission characteristics of NH3–air and NH3CH4–air combustion gas-turbine power generations. Proc Combust Inst 2017;36:3351–9.
[23] Okafor EC, Yamashita H, Hayakawa A, Somarathne KDKA, Kudo T, Tsujimura T, et al. Flame stability and emissions characteristics of liquid ammonia spray co-fired with methane in a single stage swirl combustor. Fuel 2021;287. https://doi.org/10.1016/j.fuel.2020.119433.
[24] Starikovskiy A, Aleksandrov N. Plasma-assisted ignition and combustion. Prog Energy Combust Sci 2013;39:61–110.
[25] Ju Y, Sun W. Plasma assisted combustion: Progress, challenges, and opportunities. Combust Flame 2015;162:529–32.
[26] Casey T, Han J, Belhi M, Arias P, Bisetti F, Im H, et al. Simulations of planar non-thermal plasma assisted ignition at atmospheric pressure. Proc Combust Inst 2017;36:4155–63.
[27] A. Starik, B. Loukhovitski, A. Sharipov, N. Titova, Physics and chemistry of the influence of excited molecules on combustion enhancement, Philos Trans Royal Soc A Philos T R Soc A 373 (2015), https://doi.org/10.1098/rsta.2014.0341.
[28] Mao X, Rousso A, Chen Q, Ju Y. Numerical modeling of ignition enhancement of CH4/O2/He mixtures using a hybrid repetitive nanosecond and DC discharge. Proc Combust Inst 2019;37:5545–52.
[29] Nagaraja S, Yang V, Yin Z, Adamovich I. Ignition of hydrogen–air mixtures using pulsed nanosecond dielectric barrier plasma discharges in plane-to-plane geometry. Combust Flame 2014;161:1026–37.
[30] Wang Y, Guo P, Chen H, Chen Z. Numerical modeling of ignition enhancement using repetitive nanosecond discharge in a hydrogen/air mixture I: calculations assuming homogeneous ignition. J Phys D 2020;54:1–11.
[31] Nagaraja S, Li T, Sutton J, Adamovich I, Yang V. Nanosecond plasma enhanced H2/O2/N2 premixed flat flames. Proc Combust Inst 2015;35:3471–8.
[32] Nagaraja S, Sun W, Yang V. Effect of non-equilibrium plasma on two-stage ignition of n-heptane. Proc Combust Inst 2015;35:3497–504.
[33] Snoeckx R, Jun D, Lee B, Cha M. Kinetic study of plasma assisted oxidation of H2 for an undiluted lean mixture. Combust Flame 2022;242. https://doi.org/10.1016/j.combustflame.2022.112205.
[34] Faingold G, Lefkowitz J. A numerical investigation of NH3/O2/He ignition limits in a non-thermal plasma. Proc Combust Inst 2021;38:6661–9.
[35] Faingold G, Kalitzky O, Lefkowitz J. Plasma reforming for enhanced ammonia-air ignition: a numerical study. Fuel Communications 2022;12. https://doi.org/10.1016/j.jfueco.2022.100070.
[36] Taneja TS, Johnson PN, Yang S. Nanosecond pulsed plasma assisted combustion of ammonia-air mixtures: Effects on ignition delays and NOx emissions. Combust Flame 2022;245. https://doi.org/10.1016/j.combustflame.2022.112327.
[37] Choe J, Sun W, Ombrello T, Carter C. Plasma assisted ammonia combustion: Simultaneous NOx reduction and flame enhancement. Combust Flame 2021;228:430–2.
[38] Lin Q, Jiang Y, Liu C, Chen L, Zhang W, Ding J, et al. Controllable NO emission and high flame performance of ammonia combustion assisted by non-equilibrium plasma. Fuel 2022;319. https://doi.org/10.1016/j.fuel.2022.123818.
[39] Kim G, Park J, Chung S, Yoo C. Effects of non-thermal plasma on turbulent premixed flames of ammonia/air in a swirl combustor. Fuel 2022;323. https://doi.org/10.1016/j.fuel.2022.124227.
[40] Tang Y, Xie D, Shi B, Wang N, Li S. Flammability enhancement of swirling ammonia/air combustion using AC powered gliding arc discharges. Fuel 2022;313. https://doi.org/10.1016/j.fuel.2021.122674.
[41] Shahsavari M, Konnov AA, Valera-Medina A, Jangi M. On nanosecond plasma-assisted ammonia combustion: effects of pulse and mixture properties. Combust Flame 2022;245. https://doi.org/10.1016/j.combustflame.2022.112368.
[42] Pancheshnyi S, Eismann B, Hagelaar G, Pitchford L. Computer code zdplaskin. LAPLACE, CNRS-UPS-INP, Toulouse, France: University of Toulouse; 2008.
[43] Goodwin D, Speth R, Moffat H, Weber B. Cantera: An object-oriented software toolkit for chemical kinetics, thermodynamics, and transport processes. Version 2021;2.5.1.

[44] Jangi M, Yu R, Bai XS. Development of chemistry coordinate mapping approach for turbulent partially premixed combustion. Flow Turbul Combust 2012;90:285–99.
[45] Pang K, Jangi M, Bai XS, Schramm J. Investigation of chemical kinetics on soot formation event of n-Heptane spray combustion. SAE Tech Pap 2014;1. https://doi.org/10.4271/2014-01-1254.
[46] Yang S, Nagaraja S, Sun W, Yang V. Multiscale modeling and general theory of non-equilibrium plasma-assisted ignition and combustion. J Phys D 2017;50. https://doi.org/10.1088/1361-6463/aa87ee.
[47] Han X, Wang Z, He Y, Liu Y, Zhu Y, Konnov AA. The temperature dependence of the laminar burning velocity and superadiabatic flame temperature phenomenon for NH3/air flames. Combust Flame 2020;217:314–20.
[48] Han X, Lubrano Lavadera M, Konnov AA. An experimental and kinetic modeling study on the laminar burning velocity of NH3+N2O+air flames. Combust Flame 2021;228:13–28.
[49] Konnov AA. On the role of excited species in hydrogen combustion. Combust Flame 2015;162:3755–72.
[50] Zhong H, Mao X, Rousso A, Patrick C, Yan C, Xu W, et al. Kinetic study of plasma-assisted n-dodecane/O2/N2 pyrolysis and oxidation in a nanosecond-pulsed discharge. Proc Combust Inst 2021;38:6521–31.
[51] Mao X, Chen Q, Rousso A, Chen T, Ju Y. Effects of controlled non-equilibrium excitation on H2/O2/He ignition using a hybrid repetitive nanosecond and DC discharge. Combust Flame 2019;206:522–35.
[52] Dutton database, www.lxcat.net, December 13, 2021.
[53] Manna M, Sabia P, Ragucci R, Joannon M. Oxidation and pyrolysis of ammonia mixtures in model reactors. Fuel 2020;264. https://doi.org/10.1016/j.fuel.2019.116768.
[54] Mansfield AB, Wooldridge MS. High-pressure low-temperature ignition behavior of syngas mixtures. Combust Flame 2014;161:2242–51.
[55] Mansfield AB, Wooldridge MS, Di H, He X. Low-temperature ignition behavior of iso-octane. Fuel 2015;139:79–86.
[56] Wei H, Chen C, Zhou H, Zhao W, Ren Z. Effects of turbulent mixing on the end gas auto-ignition of n-heptane/air mixtures under IC engine-relevant conditions. Combust Flame 2016;174:25–36.
[57] Wei H, Chen C, Shu G, Liang X, Zhou L. Pressure wave evolution during two hotspots autoignition within end-gas region under internal combustion engine-relevant conditions. Combust Flame 2018;189:142–54.
[58] Ombrello T, Won S, Ju Y, Williams S. Flame propagation enhancement by plasma excitation of oxygen. Part I: Effects of O3. Combust Flame 2010;157:1906–15.
[59] Sun W, Won S, Ombrello T, Carter C, Ju Y. Direct ignition and S-curve transition by in situ nano-second pulsed discharge in methane/oxygen/helium counterflow flame. Proc Combust Inst 2013;34:847–55.
[60] Samal S. Thermal plasma technology: The prospective future in material processing. J Clean Prod 2017;142:3131–50.
[61] Lefkowitz J, Guo P, Rousso A, Ju Y. Species and temperature measurements of methane oxidation in a nanosecond repetitively pulsed discharge. Philos Trans R Soc A 2015;373. https://doi.org/10.1098/rsta.2014.0333.
[62] G. Smith, D. Golden, M. Frenklach, N. Moriarty, B. Eiteneer, M. Goldenberg, C. Bowman, R. Hanson, S. Song, W. Gardiner, V. Lissianski, Z. Qin. [Online]. Available: http://www.me.berkeley.edu/gri_mech/.
[63] Shu B, Vallabhuni S, He X, Issayev G, Moshammer K, Farooq A, et al. A shock tube and modeling study on the autoignition properties of ammonia at intermediate temperatures. Proc Combust Inst 2019;37:205–11.
[64] Dai L, Gersen S, Glarborg P, Levinsky H, Mokhov A. Experimental and numerical analysis of the autoignition behavior of NH3 and NH3/H2 mixtures at high pressure. Combust Flame 2020;215:134–44.
[65] Somarathne K, Hatakeyama S, Hayakawa A, Kobayashi H. Numerical study of a low emission gas turbine like combustor for turbulent ammonia/air premixed swirl flames with a secondary air injection at high pressure. Int J Hydrog Energy 2017;42:27388–99.
[66] Okafor E, Tsukamoto M, Hayakawa A, Somarathne K, Kudo T, Tsujimura T, et al. Influence of wall heat loss on the emission characteristics of premixed ammonia-air swirling flames interacting with the combustor wall. Proc Combust Inst 2021;38:5139–46.
[67] Manna M, Sabia P, Ragucci R, Joannon M. Ammonia oxidation regimes and transitional behaviors in a Jet Stirred Flow Reactor. Combust Flame 2021;228:388–400.
[68] Sun C, Sung C, He L, Law C. Dynamics of weakly stretched flames: quantitative description and extraction of global flame parameters. Combust Flame 1999;118:108–28.
[69] Bechtold J, Matalon M. The dependence of the Markstein length on stoichiometry. Combust Flame 2001;127:1906–13.
[70] Shmakov A, Korobeinichev O, Rybitskaya I, Chernov A, Knyazkov D, Bolshova T, et al. Formation and consumption of NO in H2+O2+N2 flames doped with NO or NH3 at atmospheric pressure. Combust Flame 2010;157:556–65.
[71] Wolk B, DeFilippo A, Chen J, Dibble R, Nishiyama A, Ikeda Y. Enhancement of flame development by microwave-assisted spark ignition in constant volume combustion chamber. Combust Flame 2013;160:1225–34.